BÜLOW, R., NEUBÜSER, J. & WONDRATSCHEK, H. (1971). *Acta Cryst.* A27, 520-523.
HERMANN, C. (1949). *Acta Cryst.* **2**, 139-145.
NEUBÜSER, J., WONDRATSCHEK, H. & BÜLOW, R. (1971). *Acta Cryst.* A27, 517-520.
SMAALEN, S. VAN, BRONSEMA, K. D. & MAHY, J. (1986). *Acta Cryst.* B42, 43-50.
VEYSSEYRE, R., PHAN, TH. & WEIGEL, D. (1985). *C. R. Acad. Sci.* **300**, 51-54.
WEIGEL, D., PHAN, TH. & VEYSSEYRE, R. (1984). *C. R. Acad. Sci.* **298**, 825-828.
WEIGEL, D., PHAN, TH. & VEYSSEYRE, R. (1987). *Acta Cryst.* A43, 294-304.
WEIGEL, D. & VEYSSEYRE, R. (1982). *C. R. Acad. Sci.* **295**, 317-322.
WEIGEL, D., VEYSSEYRE, R., PHAN, TH., EFFANTIN, J. M. & BILLIET, Y. (1984). *Acta Cryst.* A40, 323-330.
WOLFF, P. M. DE (1974). *Acta Cryst.* A30, 777-785.
WOLFF, P. M. DE, JANSSEN, T. & JANNER, A. (1981). *Acta Cryst.* A37, 625-636.
WONDRATSCHEK, H., BÜLOW, R. & NEUBÜSER, J. (1971). *Acta Cryst.* A27, 523-535.

Acta Cryst. (1989). A**45**, 193-199

Modified Multislice Theory for Calculating the Energy-Filtered Inelastic Images in REM and HREM

BY Z. L. WANG

Cavendish Laboratory, University of Cambridge, Madingley Road, Cambridge CB3 0HE, England

(*Received* 7 *March* 1988; *accepted* 27 *September* 1988)

Abstract

Inelastic plasmon diffuse scattering (PDS) is treated as an effective position-dependent potential perturbing the incident electron wavelength in a solid surface, resulting in an extra phase grating term in the slice transmission function. This potential is derived for the geometry of reflection electron microscopy (REM) and high-resolution electron microscopy (HREM). The energy-filtered inelastic images can be calculated following the routine image simulation procedures by using different slice transmission functions for the elastic and inelastic waves, by considering the 'transitions' of the elastic scattered electrons to the inelastic scattered electrons. It is predicted that the inelastic scattering could modify the electron intensity distribution at a surface. It is possible to take high-resolution energy-filtered inelastic images of crystals, the resolution of which is about the same as that taken from the elastic scattered electrons.

1. Introduction

Multislice theory has been successfully applied in image simulation for high-resolution electron microscopy (HREM). Recently, this theory has been modified for calculating the image contrast and electron resonance processes at a crystal surface in the geometry of reflection electron microscopy (REM) or reflection high-energy electron diffraction (RHEED). Contrast variations of an atomic surface step under different focusing conditions were interpreted (Peng & Cowley, 1987). Surface-layer resonance properties under resonance conditions were simulated; the generating processes of reflection waves at an atomic flat surface and a surface with a step up or down were investigated and compared with REM observations (Wang, Lu & Cowley, 1987; Wang, 1988). All these calculations, however, were based on elastic scattering theory. In the REM case, most of the incident electrons have lost the energy of the surface plasmon during the scattering (Wang & Cowley, 1988), and the calculated results from the elastic theory cannot represent the real interaction behavior of the electrons with surfaces. A new theory which includes the effects of electron inelastic scattering in the dynamical calculations is required for quantitative analysis of REM and RHEED data. This situation also happens in HREM if a sample is thicker than the inelastic mean free path of the electrons.

Recently Wang & Lu (1988) have suggested a new method, from which the plasmon diffuse scattering (PDS) can be included in the calculation of the multislice theory. The energy loss of the electrons due to plasmon excitations was characterized by an effective potential modifying the kinetic energy of the incident electrons, and resulting in a perturbation to the electron wavelength. The phase grating function of each slice is the product of an elastic with an inelastic function arising from the plasmon losses. Thus multiple excitations of plasmons were automatically involved in the calculations.

In this paper, as a continuation of our previous work (Wang & Lu, 1988), (1) the relativistic dielectric response theory will be employed to calculate the electron energy loss rate and its associated perturbation effect on the slice transmission function (STF); (2) the quantum-mechanical basis of this method will be addressed; (3) a modified multislice theory for

0108-7673/89/020193-07$03.00

simulating the energy-filtered inelastic images for REM and HREM will be presented; (4) the effects of the angular distribution of inelastic scattering will be introduced in the multislice calculations; and, finally, (5) calculations for GaAs (110) will be used to demonstrate the importance of the PDS for image simulations in REM.

2. Plasmon diffuse scattering in dynamical calculations for REM and HREM

Plasmon diffuse scattering (PDS), thermal diffuse scattering (TDS) and single-electron excitations are the three main inelastic scattering processes in electron diffraction. A detailed treatment of TDS in dynamical calculations has been given by Cowley (1981, 1988*a*). Since the scattering cross section of single-electron excitation is much smaller than that of plasmons, the contribution to the electron images can be neglected. Thus the main inelastic scattering process which needs to be addressed in the dynamical calculation is the PDS.

To derive the modified from of the slice transmission function, the total energy loss of an electron due to plasmon excitations needs first to be considered. Starting from a planar interface formed by two semi-infinite large media a and b, in the relativistic dielectric excitation theory (*e.g.* Garcia-Molina, Gras-Marti, Howie & Ritchie, 1985), a point electron travelling in medium b at distance x parallel to an interface with medium a has a differential probability per unit distance for energy loss ($\hbar\omega$) and momentum transfer ($\hbar q_y$), in the direction parallel to the interface and normal to the moving direction, given by

$$\frac{\mathrm{d}^2P(\omega, q_y, x)}{\mathrm{d}\omega\,\mathrm{d}q_y}=\frac{e^2}{2\pi^2\varepsilon_0\hbar v^2}\,\mathrm{Im}\left[F(q_y, x)-\frac{1-\beta^2\varepsilon_b}{\varepsilon_b\alpha_b}\right], \tag{1}$$

where $\beta = v/c$, $\alpha_{a,b}^2 = q_y^2+(\omega/v)^2(1-\beta^2\varepsilon_{a,b})$, v is the velocity of the electron, and ε_a and ε_b are the dielectric constants of media a and b. The quantity $F(q_y, x)$ in (1) is given by

$$F(q_y, x)=\left[\frac{2\alpha_b^2(\varepsilon_a-\varepsilon_b)}{\varepsilon_a\alpha_b+\varepsilon_b\alpha_a}+(\alpha_a-\alpha_b)(1-\varepsilon_b\beta^2)\right]\times\frac{\exp(-2\alpha_b|x|)}{\varepsilon_b\alpha_b(\alpha_a+\alpha_b)}. \tag{2}$$

The total energy loss of the electron while travelling a distance z is

$$\Delta E(x, z)=\int_0^z \mathrm{d}z\int_0^\infty \mathrm{d}\omega\int_0^{q_c}\mathrm{d}q_y\,\hbar\omega\,\mathrm{d}^2P(\omega, q_y, x)/\mathrm{d}\omega\,\mathrm{d}q_y. \tag{3}$$

Here z is a function of x, depending on the scattering trajectory of the electron (Howie, Milne & Walls, 1985). The integration $\mathrm{d}q_y$ covers various momentum transfers ($\hbar q_y$) parallel to the interface and normal to the beam direction with an upper limit set by some specimen-dependent cut off. The inelastic mean free path of the electron is defined as

$$1/\Lambda(x)=\int_0^\infty \mathrm{d}\omega\int_0^{q_c}\mathrm{d}q_y\,\mathrm{d}^2P(\omega, q_y, x)/\mathrm{d}\omega\,\mathrm{d}q_y; \tag{4a}$$

the associated absorption coefficient is

$$\mu(x)=1/\Lambda(x). \tag{4b}$$

In the multislice theory, a crystal is treated as a 'fixed' distribution of atomic potential wells. The total structural energy of the crystal is assumed not to be influenced by the incident beam. There is no energy transfer from the crystal to the incident beam. Then the total energy of the electron can be written as

$$E=P^2/2m+[-eU_a(x, y, z)]+\Delta E(x, z). \tag{5}$$

The first term is the kinetic energy of the electron. The second term is the potential energy of the electron in the crystal potential field (U_a). The third term is the total energy loss of the electron due to plasmon excitations, which is essentially the energy transferred from the electron to the plasmon oscillators. For fast electrons, the last two terms in (5) are much smaller than the kinetic energy (100 keV) of the electron and can be considered as small perturbations. The total energy of the electron can be taken approximately as its kinetic energy.

To find the perturbation result of ΔE on the scattering of electrons in a solid, one starts from the Schrödinger equation

$$[-(\hbar^2/2m)\nabla^2-eU_a(x, y, z)+\Delta E(x, z)]\varphi=E\varphi \tag{6}$$

to derive the phase grating function of a thin potential slice. For fast incident electrons, φ can be written in the form $\psi\exp(i\mathbf{K}.\mathbf{r})$, where $\mathbf{K}$ is the incident electron wave vector. After making the approximation $|\nabla^2\psi|\ll|2\mathbf{K}.\nabla\psi|$ (Hirsch, Howie, Nicholson, Pashley & Whelan, 1977), one can write (6) as

$$(\hbar^2/2m)[K^2\psi-i2\mathbf{K}.\nabla\psi]+(-eU_a+\Delta E)\psi=E\psi. \tag{7}$$

Since $E\simeq\hbar^2K^2/2m\simeq eV_0$, $|K_x|\ll|K_z|$, $|K_y|\ll|K_z|$ and $K_z\simeq K_0$, then (7) can be written in the form

$$-i(\hbar^2K_0/m)\,\partial\psi/\partial z\simeq(eU_a-\Delta E)\psi. \tag{8}$$

The electron wave (ψ_0), after being scattered by a thin potential slice Δz, is given by

$$\psi=\psi_0\exp\left[i\sigma\int_0^{\Delta z}(U_a+U_{ef})\,\mathrm{d}z\right], \tag{9a}$$

where $\sigma=\pi/\lambda_0V_0$. λ_0 is the wavelength of the initial incident electron with energy $E_0=eV_0$. U_{ef} is an

effective potential for characterizing the PDS.

$$U_{ef} = -\Delta E(x, z)/e$$
$$= -(1/e)\int_0^z dz \int_0^\infty d\omega \int_0^{q_c} dq_y\, \hbar\omega \times d^2P(\omega, q_y, x)/d\omega\, dq_y. \quad (9b)$$

Equation (9a) is the result of the phase-object approximation. It is a basic equation of the multislice theory. The modified transmission function for the nth slice can then be written as

$$q_n = \exp(i\sigma U_a \Delta z) \exp(i\sigma U_{ef} \Delta z). \quad (10a)$$

The first term is the phase-grating result of the crystal potential, which is the same as that in the original multislice theory (Cowley & Moodie, 1957). The second term is a phase perturbation function arising from the inelastic PDS. The electron wave function, after being scattered by the nth slice, can be written as (Cowley & Moodie, 1957)

$$\psi_n = (\psi_{n-1} q_n) * P_n, \quad (10b)$$

with P_n as the propagation function of the nth slice for the electrons with energy E_0,

$$P_n = (i/\Delta z \lambda_0) \exp[-iK(x^2+y^2)/2\Delta z]. \quad (10c)$$

3. Modified multislice theory for calculating the energy-filtered inelastic images

Calculated results of (10a) to (10c) give the total contributions of the elastic and inelastic scattering to the electron images. In practical analysis, it is desirable to obtain the energy-filtered inelastic high-resolution images to compare with the experimental observations (Hashimoto, 1985). However, there is no proper theory available for simulating the inelastic images. The purpose of this section, based on the theory in § 2, is to introduce a modified multislice approach for calculating the inelastic images in REM and HREM.

We select a narrow energy filter that allows only those electrons which have lost the energy of a *single* plasmon (E_p) in the energy range $E_p - \Delta/2 < \Delta E < E_p + \Delta/2$ to pass. The energy window (Δ) is selected so small that the electrons which pass through the filter can be considered as a monoenergetic stream with kinetic energy $E_0 - E_p$. The other electrons with different energy losses are assumed to be 'absorbed' by the filter. The part that needs to be considered represents the 'transitions' of the eleastic scattered electrons (with energy E_0) to the inelastic scattered electrons which have lost the energy in the window range. The propagation of these electrons in the crystal after being selected by the window is reclassified as 'elastically' scattered; otherwise they will be 'absorbed' by the filter. The propagation of these filtered electrons from different slices having energy $E_0 - E_p$ is treated as coherent (Doyle, 1971). In this case, calculations based on coherent interference do not differ significantly from calculations based on incoherent interference if the sample is thick (Cowley, 1988b). This is because the sum of the waves from a large number of slices averages out their interference effects.

If q_n^e is defined to represent the elastic scattering of the crystal potential U_a, and q_n^i is defined to characterize the generation of an inelastic wave from the nth potential slice, with a probability $\Delta z/\Lambda(x, \Delta)$, then

$$q_n^e = \exp(i\sigma U_a \Delta z); \quad (11a)$$
$$q_n^i = \exp[i\sigma(U_a \Delta z)] \exp[i\sigma U_{ef}(\Delta)\Delta z] \times [\Delta z/\Lambda(x, \Delta)]^{1/2}. \quad (11b)$$

Here $U_{ef}(\Delta)$ is defined in (9b) except that the integration limits of ω are replaced by $E_p - \Delta/2$ and $E_p + \Delta/2$ in order to specify the selection range of the energy filter. The term $\exp[i\sigma U_{ef}(\Delta)\Delta z]$ is added in (11b) to indicate the average phase shift due to the energy loss according to (10a). The introduction of the factor $(\Delta z/\Lambda)^{1/2}$ in (11b) is analogous to the treatment of the transmission electron microscopy case (Doyle, 1971), which indicates the generation of the plasmon diffuse scattering from the nth slice. The electron mean free path Λ for the energy-window range considered is

$$1/\Lambda(x, \Delta) = \int_{E_p-\Delta/2}^{E_p+\Delta/2} d\omega \int_0^{q_c} dq_y\, d^2P(\omega, q_y, x)/d\omega\, dq_y. \quad (11c)$$

If we assume that an electron wave (ψ_0) is incident on the first slice along the z direction, the wave after penetrating this slice, according to (10b) and (11), would be

$$\psi_1^e = [\psi_0 q_1^e \exp(-\mu \Delta z/2)] * P_1^e; \quad (12a)$$
$$\psi_1^i = [\psi_0 q_1^i \exp(-\mu \Delta z/2)] * P_1^i. \quad (12b)$$

Here ψ_1^e is used to characterize the elastic scattered wave; ψ_1^i is used to characterize the new generated inelastic wave. The term $\exp(-\mu \Delta z/2)$ is added to introduce the absorption effect of the multiple PDS (Cowley, 1981). μ is defined in (4a). In (12), P_n^e and P_n^i are the propagation functions for the elastic (with energy E_0) and inelastic (with energy $E_0 - E_p$) scattered electrons respectively, as defined in (10c).

In practical electron energy-loss experiments, the plasmon peak is relatively sharp compared with the other intensities with energy loss lower than E_p, especially for metals and semiconductors. Based on this fact, the probability of electron scattering with energy loss $\hbar\omega < E_p - \Delta/2$ is much smaller than that of elastic scattering while propagating through a distance Δz. Then the probability of having a double inelastic process, first losing energy $\hbar\omega$ then losing energy $E_p - \hbar\omega$, is very small compared with that of

having one inelastic process with energy loss E_p while penetrating a slice. Thus one does not need to consider the multiple scattering of the electrons with energy loss $\hbar\omega < E_p - \Delta/2$ back into the window. In other words, 'transitions' of electrons with energy loss $\hbar\omega$ ($<E_p - \Delta/2$) to electrons with energy loss in the window range, during the propagation through a slice, can be neglected. Electrons which have the possibility of losing double the energy of the plasmon would be absorbed by the filter. Therefore, the wave function after penetrating the second slice can be written as

$$\psi_2^e = [\psi_1^e q_2^e \exp(-\mu\Delta z/2)] * P_2^e; \quad (13a)$$

$$\psi_2^i = [(\psi_1^i q_2^e + \psi_1^e q_2^i) \exp(-\mu\Delta z/2)] * P_2^i; \quad (13b)$$

ψ_2^e is the continuous elastic propagation of the 'old' elastic wave from the first slice. ψ_2^i is a summation of the elastic transmitted 'old' inelastic wave from the first slice and the new generated inelastic wave from the second slice. Following the same procedures, we write the wave function of the electrons after being scattered by the nth ($n>2$) slice as

$$\psi_n^e = [\psi_{n-1}^e q_n^e \exp(-\mu\Delta z/2)] * P_n^e; \quad (14a)$$

$$\psi_n^i = [(\psi_{n-1}^i q_n^e + \psi_{n-1}^e q_n^i) \exp(-\mu\Delta z/2)] * P_n^i. \quad (14b)$$

Equation (14a) describes the elastic transmission of an elastic scattered wave through the nth slice. In (14b), the first term is the result of the elastic transmission of the inelastic scattered wave through the nth slice. The second term is the new 'generated' inelastic wave from the nth slice, arising from the 'transition' of the elastic wave to the inelastic wave.

After penetration of the crystal (Nth slice), one may evaluate the time average over the phases of the elastic and inelastic scattered waves to give the intensity distribution in the energy-filtered inelastic images as

$$I^i = |\psi_N^i / N^{1/2}|^2. \quad (15)$$

A factor $N^{1/2}$ is added in order to normalize the inelastic scattering intensity according to the Poisson distribution to that in transmission electron microscopy (Doyle, 1971). The intensity of the pure elastic-scattered electrons is given by

$$I^e = |\psi_N^e|^2. \quad (16)$$

Throughout the above discussion, it can be seen that the calculation of the energy-filtered inelastic images is similar to the routine image simulation for HREM. However, the two 'interacting' waves, the elastic scattered wave and the inelastic scattered wave, need to be calculated through different slice transmission functions by considering the 'transitions' of the elastic electrons to the inelastic electrons. Equations (11) to (14) are the equations for calculating the energy-filtered inelastic images of single-plasmon-loss electrons. Adequate theory can be derived for the energy-filtered double plasmon images by considering the 'extra transitions' of the electrons which have lost a single plasmon energy to the electrons which have lost double the energy of the plasmon.

One thing we must emphasize here is that the calculation of the inelastic scattering in the geometry of RHEED has to consider the generation of the inelastic scattering while the electrons are travelling in the vacuum. This is equivalent to introducing an incident wave for the inelastic scattering, which should be added coherently to the final wave $\psi_N^i / N^{1/2}$ in (15). A detailed introduction to this is given elsewhere (Wang, 1989a, b).

4. Modifications of the inelastic angular distribution to the effective potential U_{ef}

A method of introducing the PDS in the multislice theory was given in § 2. The effective potential defined there was derived from the inelastic non-deflection approximation. In fact, large-angle inelastic scattering can make a significant contribution to the formation of diffuse scattering in RHEED, particularly to Kikuchi patterns (Okamoto, Ichinokawa & Ohtsuki, 1971). This section discusses the effect of the inelastic angular distribution on the calculation of U_{ef}. Since $\sigma\Delta z U_{ef}$ is very small, (10b) can be written as

$$\psi_n(x, y) = \{\psi_{n-1}(x, y) q_n^e(x, y) \times [1 + i\sigma\Delta z U_{ef}(x, y, z)]\} * P_n(x, y). \quad (17)$$

By using Fourier transformation, in the two-dimensional reciprocal space $\mathbf{u} = (u_x, u_y)$, one can modify (17) to

$$\psi_n(\mathbf{u}) = [\psi_{n-1}(\mathbf{u}) * q_n^e(\mathbf{u}) + i\sigma\Delta z \psi_{n-1}(\mathbf{u}) * U_{ef}(\mathbf{u}, z) * q_n^e(\mathbf{u})] P_n(\mathbf{u}). \quad (18a)$$

with

$$U_{ef}(\mathbf{u}, z) = -\Delta E(\mathbf{u}, z)/e. \quad (18b)$$

To include the inelastic angular broadening effect in the dynamical calculations the physical meaning of $U_{ef}(\mathbf{u}, z)$ needs to be clarified. In (18a), the first term represents the elastic scattering of the incident beams in the nth slice. The second term is the result of inelastic angular broadening on the transmitted beams. The angular distribution of this term is related to the angular distribution of the PDS covering various energy losses. Equation (18b) can be understood as an effective potential due to various energy losses while being scattered in a particular direction $\mathbf{u}$ during travel through distance z, *i.e.*

$$U_{ef}(\mathbf{u}, z) = -\frac{1}{e} \int_0^z \mathrm{d}z \int_0^\infty \mathrm{d}\omega\, \hbar\omega \left. \frac{\mathrm{d}^2 P(\omega, \mathbf{q})}{\mathrm{d}\omega\, \mathrm{d}q_x\, \mathrm{d}q_y} \right|_{\mathbf{q}=2\pi\mathbf{u}}. \quad (19)$$

In other words, (19) can be interpreted as the effective potential arising from the inelastic scattering by definite momentum transfer $\hbar\mathbf{q}$ ($=2\pi\hbar\mathbf{u}$) for various energy losses. Turning (19) back to real space, one obtains

$$U_{ef}(x, y, z) = -\frac{1}{e}\int_0^z dz \int_0^\infty d\omega\, \hbar\omega \int d\mathbf{q} \exp(-i\boldsymbol{\rho}\cdot\mathbf{q}) \times \frac{d^2P(\omega, \mathbf{q})}{d\omega\, dq_x\, dq_y}. \quad (20a)$$

Equation (20a) is a general expression for the effective potential. The analytical expression of U_{ef} for the REM and HREM cases will be derived in the next section. Similar results can be derived for $\Lambda(\boldsymbol{\rho})$:

$$\frac{1}{\Lambda} = \int_0^\infty d\omega \int d\mathbf{q} \exp(-i\boldsymbol{\rho}\cdot\mathbf{q}) \frac{d^2P(\omega, \mathbf{q})}{d\omega\, dq_x\, dq_y} \quad \boldsymbol{\rho} = (x, y). \quad (20b)$$

4.1. *U_{ef} in REM and RHEED geometry*

In the geometry of REM and RHEED using (1) and considering the momentum transfer q_y at position x in (19) one can obtain for U_{ef} the expression

$$U_{ef}(x, y, z) = \frac{e}{2\pi^2\varepsilon_0 v^2}\int_0^z dz \int_0^{q_c} dq_y \cos(q_y y) \times \int_0^\infty d\omega\, \mathrm{Im}\left[F(q_y, x) - \frac{1-\beta^2\varepsilon_b}{\varepsilon_b\alpha_b}\right]\omega. \quad (21)$$

Equation (21) is a new modified effective potential for the REM case. It is easy to see that by taking $y = 0$, (21) becomes (9b). The only difference between (21) and (9b) is that a Fourier transform factor $\cos(q_y y)$ has been added in (21). By using (21) the angular distribution of the inelastic scattering will be included in the dynamical calculations.

4.2. *U_{ef} for transmission HREM*

In transmission HREM, all the incident electrons can be considered to travel approximately the same distance through a sample provided it is a thin foil. The main excitation process in a solid is the volume plasmon oscillation. By using Ritchie's (1957) results, one obtains the excitation probability for the volume plasmon per unit path length of energy loss ($\hbar\omega$) and momentum transfer ($\hbar\mathbf{q}$) as

$$\frac{d^2P(\omega, \mathbf{q})}{d\omega\, dq_x\, dq_y} = \frac{e^2}{4\pi^3\varepsilon_0\hbar v^2}\frac{1}{q^2+(\omega/v)^2}\mathrm{Im}\left(-\frac{1}{\varepsilon}\right). \quad (22)$$

By using (20), one gets

$$U_{ef}(\rho, z) = \frac{ze}{2\pi^2\varepsilon_0 v^2}\int_0^\infty d\omega \int_0^{q_c} dq \frac{J_0(q\rho)q}{q^2+(\omega/v)^2}\mathrm{Im}\left(\frac{1}{\varepsilon}\right)\omega. \quad (23)$$

$J_0(q\rho)$ is the zero-order Bessel function. By taking the limit of non-deflected scattering (or very small-angle scattering) in (23), *i.e.* $\rho \simeq 0$, U_{ef} becomes the total energy lost by the electron for various momentum transfers due to plasmon excitations. For the simple free-electron-model case, the half width of the plasmon angular distribution in reciprocal space is about $\omega_p/2\pi v$ from (23), where ω_p is the plasmon energy. The half width of U_{ef} in real space is approximately $2\pi v/\omega_p \simeq 450$ Å for $\omega_p = 15$ eV and $E_0 = 100$ keV. This tells us that U_{ef} is a very slowly varying function of $\rho = (x^2+y^2)^{1/2}$, which will not affect the resolution of the image according to (11b). This indicates that the resolution of the images taken with the energy-filtered inelastic electrons is the same as for those taken with the elastic-scattered electrons. This prediction is in agreement with Cowley's conclusion and has been verified in HREM experiments (Hashimoto, 1985).

5. Application to GaAs (110) surface

The theory presented in § 2 has been applied to a GaAs (110) surface to demonstrate the perturbation result of the PDS on the electron distribution at a crystal surface. The calculated effective potential U_{ef} and the absorption coefficient μ from (3) and (4b) are shown in Figs 1 and 2. U_{ef} was calculated based on the assumption that the electrons are moving parallel to the surface. The total energy loss of the electrons is the product of its travelling distance and its energy-loss rate. An important feature shown in Fig. 1 is that the effective potential varies sharply only when the electron beam approaches the surface ($x = 0$). This indicates that PDS plays a dominate role in RHEED. In this case, the modulation effect of the effective potential U_{ef} in the phase grating function [q_n^i in (11b)] becomes important. This shows that the inelastic scattering could totally affect the scattering behavior of the electrons at a crystal surface, resulting in a perturbation to the image contrast in REM.

In order to show the effect of PDS on the electron propagation at a crystal surface, one calculates the electron density distribution at the same thickness under the same incident conditions with and without considering the PDS in the slice transmission function. By using the modulated form of the STF in (10a), one compares the calculated results for the three cases: (1) elastic scattering with no absorption (left column of Fig. 3); (2) elastic scattering plus plasmon inelastic effect with no absorption (middle

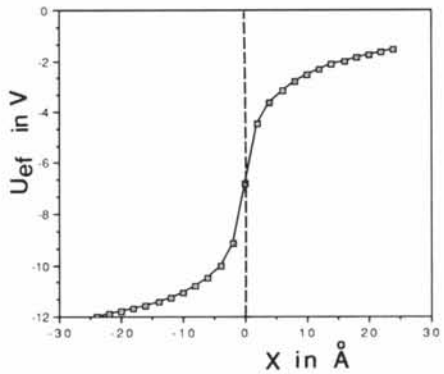

Fig. 1. Calculated effective potential U_{ef} according to equation (9*b*) for GaAs surface, as a function of the electron excitation position x ($x>0$ in vacuum; $x<0$ in crystal), after travelling distance $z=1000$ Å. With beam energy 100 keV, $q_c=1$ Å^{-1}. The dashed line represents the position of the surface.

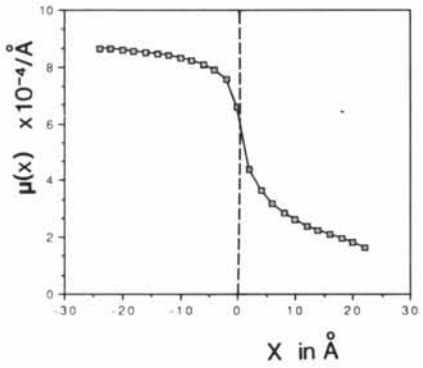

Fig. 2. Calculated absorption coefficient according to equation (4*b*) for GaAs surface, as a function of electron excitation positions ($x>0$ in vacuum; $x<0$ in crystal). Beam energy 100 keV, $q_c=1$ Å^{-1}. The dashed line represents the position of the surface.

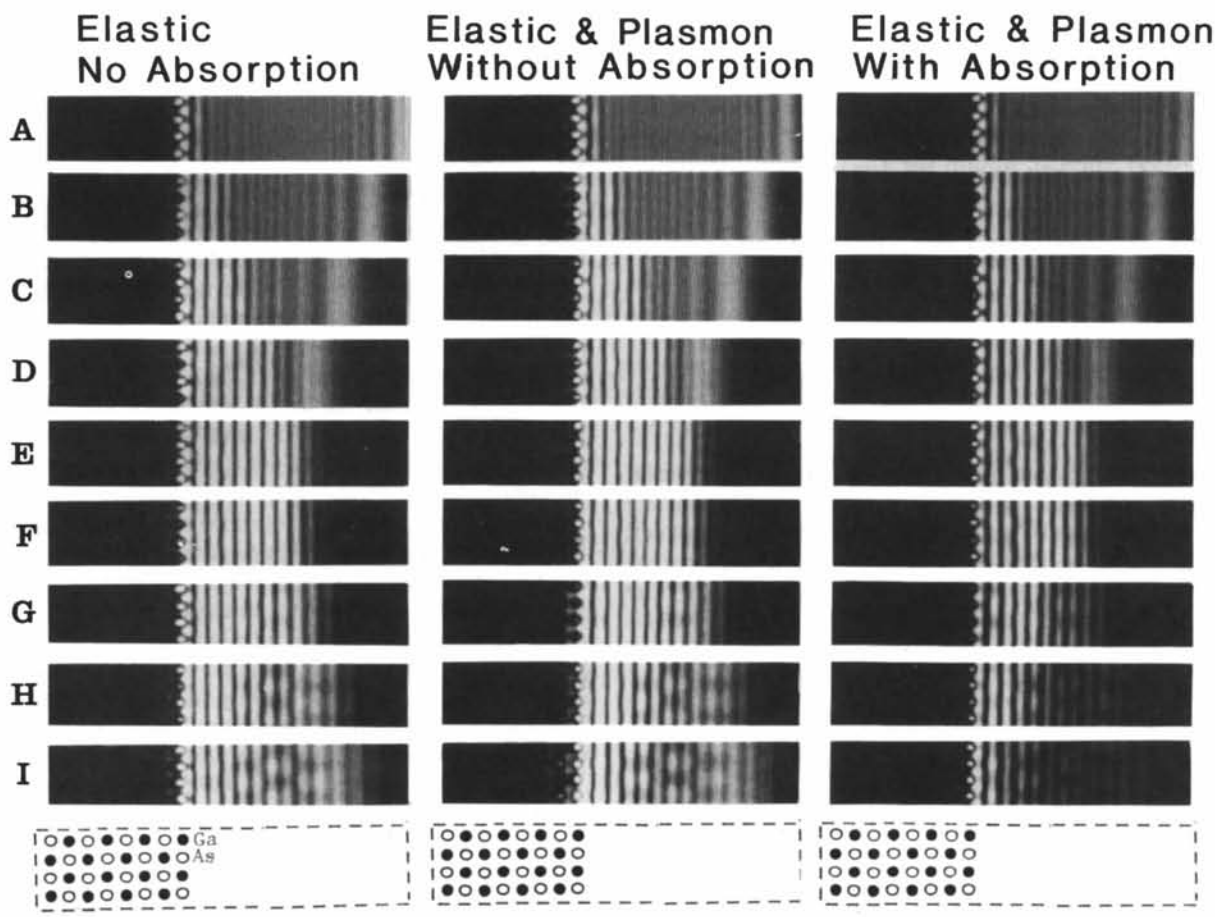

Fig. 3. Dynamical calculated electron intensity distributions near to the GaAs (110) surface by using the theories for elastic scattering with no absorption (left column), elastic plus plasmon inelastic effect without absorption (middle column) and elastic plus plasmon inelastic effect with absorption (right column), at thicknesses (*A*) 226, (*B*) 452, (*C*) 678, (*D*) 904, (*E*) 1130, (*F*) 1356, (*G*) 1582, (*H*) 1808 and (*I*) 2034 Å. With beam energy 100 keV, beam azimuth [001], incident angle 12 mrad and beam width $b=30$ Å. The intensity is output in the beam cross section with the beam going into the paper.

column of Fig. 3); and (3) elastic scattering plus plasmon inelastic effect with absorption (right column of Fig. 3). A monoenergetic electron beam with energy 100 keV and beam width $b = 30$ Å was selected to strike the surface at a glancing angle of 12 mrad, corresponding to the 440 specular reflection of GaAs. The slice thickness was chosen as $\Delta z = 2{\cdot}827$ Å. The calculated results were output in a plane perpendicular to the beam at different propagation distances. A detailed introduction to the calculation method has been given elsewhere (Wang *et al.*, 1987).

Fig. 3 shows the calculated electron density distributions at the surface for the three cases. Comparison between the intensity output in the left and the middle columns does not show any obvious difference from rows (*A*) to (*C*). This indicates that the PDS cannot affect the image contrast significantly if the sample is thin ($t < 600$ Å). Thus, the 'safety' thickness in simulating the REM images by using the elastic multislice theory is about $t < 600$ Å for GaAs. If the electron propagation distance is longer than 600 Å, the influence of the PDS needs to be taken into account. The interference results of the incident wave with the reflection wave can be observed in the region of bright intensity fringes. The effect of the PDS at the surface is to spread out the electron distribution around the atomic columns, resulting in an intensity redistribution between the surface potential barrier and the first atomic layer [see Fig. 3 (*G*)]. The electrons have been scattered closer to the surface in the vacuum and further away from the surface inside the crystal [see Fig. 3 (*I*), left and middle columns]. This is in agreement with the expected results from Fig. 1, because the electrons are tending to flow to the places which have the lowest potential energies.

The absorption effect of the PDS can significantly limit the plasmon diffuse scattering (see right column in Fig. 3). The scattered electrons between the atomic columns are absorbed during the propagation. The main electron beam is still distributed along atomic columns. This is due to electron channelling. As noticed in Fig. 2 μ increases as the electron goes into the surface. This effect limits the penetration depth of the electrons, and it improves the surface structural sensitivity of the REM (Wang & Lu, 1988).

This paper has concentrated on the presentation of the modified multislice theory for calculating the energy-filtered inelastic images. It is also possible to use (10) to calculate the total contributions of the elastic and inelastic electrons, with energy-loss range from 0 to ∞, to the REM images. The incident wave can be divided into many narrow streams, so that each of them can be considered as a monoenergetic beam during the propagation. Propagation of each stream is governed by (10*a*) to (10*c*). The final diffraction results of the beam can be obtained from the summation of all these streams. By dividing the incident wave into many small streams, the corresponding electron feed-in problem in the REM geometry can be solved. All these calculations are reported elsewhere (Wang, 1989*a*, *b*).

Based on the theory presented in § 3, the energy-filtered inelastic single-electron-excitation images can be simulated. The difference is in the use of the core-shell differential excitation cross section in the calculation of U_{ef}. With the improvement of modern electron microscopy techniques, it may be possible in the future to get inelastic core-shell high-resolution images.

The author is grateful to Professor J. M. Cowley for some critical discussions. Thanks to Mr Ping Lu for calculating Fig. 3.

References

COWLEY, J. M. (1981). *Diffraction Physics.* Amsterdam: North-Holland.

COWLEY, J. M. (1988*a*) *Acta Cryst.* A**44**, 847-853.

COWLEY, J. M. (1988*b*). Private communication.

COWLEY, J. M. & MOODIE, A. F. (1957). *Acta Cryst.* **10**, 609-619.

DOYLE, P. A. (1971). *Acta Cryst.* A**27**, 109-116.

GARCIA-MOLINA, R., GRAS-MARTI, A., HOWIE, A. & RITCHIE, R. H. (1985). *J. Phys. C*, **18**, 5335-5348.

HASHIMOTO, H. (1985). *Ultramicroscopy*, **18**, 19-32.

HIRSCH, P., HOWIE, A., NICHOLSON, R. B., PASHLEY, D. W. & WHELAN, M. J. (1977). *Electron Microscopy of Thin Crystals*, § 9.6. London: Butterworths.

HOWIE, A., MILNE, R. H. & WALLS, M. G. (1985). *Inst. Phys. Conf. Ser.* No. 78, pp. 117-120.

OKAMOTO, K., ICHINOKAWA, T. & OHTSUKI, Y.-H. (1971). *J. Phys. Soc. Jpn*, **30**, 1690-1701.

PENG, L. M. & COWLEY, J. M. (1987). *Acta Cryst.* A**42**, 545-552.

RITCHIE, R. H. (1957). *Phys. Rev.* **106**, 874-881.

WANG, Z. L. (1988). *Ultramicroscopy*, **24**, 371-386.

WANG, Z. L. (1989*a*). *Surf. Sci.* Submitted.

WANG, Z. L. (1989*b*). *Surf. Sci.* Submitted.

WANG, Z. L. & COWLEY, J. M. (1988). *J. Microsc. Spectrosc. Electron. (Paris)*, **13**, 189-204.

WANG, Z. L. & LU, P. (1988). *Ultramicroscopy*, **26**, 217-226.

WANG, Z. L., LU, P. & COWLEY, J. M. (1987). *Ultramicroscopy*, **23**, 205-222.